tributed yielding mechanisms, such as granular flow (*5*, *6*) or velocity-strengthening slip along pervasively distributed fractures (*27*). Distributed yielding is commonly expressed along faults as fault-related folds, rock fabrics, topographic uplift, and gradients in cumulative slip and slip-rate (*8*, *28*–*30*). The time scale of this distributed yielding could be essentially coseismic or take months, and it may be difficult to distinguish from other coseismic deformation. Postseismic dilatancy recovery (*6*) could provide indirect evidence of its occurrence.

If a substantial fraction of plate-boundary motion is absorbed as distributed deformation in zones of structural complexity, surface rupture and strong ground motion hazard may be underpredicted. Paleoseismic measurements will underestimate fault slip rates at depth due to this unaccounted deformation. In addition to slip rate, maximum earthquake size may also be misjudged due to incomplete knowledge of the linkages between faults. These problems modestly affect hazard from fast-slipping, well-localized primary plate-boundary faults but can lead to severe underestimation of hazard away from primary faults where large ($>M_w$ 7) earthquakes along secondary fault arrays dominate strong ground motions (*1*). As exemplified by the highly segmented El Mayor–Cucapah surface rupture and similarly sized historic events in southern California (*9*–*11*), anticipating the sizes of the largest earthquakes along secondary fault arrays and the shaking and rupture hazards that these pose to critical facilities and lifelines requires careful attention to the extent and connectivity of mapped active faults. Scarp-forming paleoearthquakes along short fault segments, accompanied by large along and off-fault strains, provide key hazard information, as such events probably involved adjacent fault segments as parts of a larger surface rupture.

References and Notes

1. P. England, J. Jackson, *Nat. Geosci.* **4**, 348 (2011).
2. R. Harris, S. Day, *Geophys. Res. Lett.* **26**, 2089 (1999).
3. S. G. Wesnousky, *Nature* **444**, 358 (2006).
4. G. King, S. Wesnousky, *Bull. Seismol. Soc. Am.* **97**, 1833 (2007).
5. Y. Fialko, D. Sandwell, M. Simons, P. Rosen, *Nature* **435**, 295 (2005).
6. E. J. Fielding, P. R. Lundgren, R. Bürgmann, G. J. Funning, *Nature* **458**, 64 (2009).
7. W. Huang, A. Johnson, *J. Geophys. Res.* **115**, B03408 (2010).
8. E. Shelef, M. Oskin, *J. Geophys. Res.* **115**, B05308 (2010).
9. K. Mueller, T. Rockwell, *Bull. Geol. Soc. Am.* **107**, 8 (1995).
10. K. Sieh *et al.*, *Science* **260**, 171 (1993).
11. J. Treiman, K. Kendrick, W. Bryant, T. Rockwell, S. McGill, *Bull. Seismol. Soc. Am.* **92**, 1171 (2002).
12. J. Liu-Zeng *et al.*, *Bull. Seismol. Soc. Am.* **100**, 2615 (2010).
13. P. Haeussler *et al.*, *Bull. Seismol. Soc. Am.* **94**, S23 (2004).
14. Y. Klinger *et al.*, *Bull. Seismol. Soc. Am.* **95**, 1970 (2005).
15. M. Berberian *et al.*, *Geophys. J. Int.* **136**, 671 (1999).
16. E. Hauksson *et al.*, *Pure Appl. Geophys.* **168**, 1255 (2011)
17. S. Wei *et al.*, *Nat. Geosci.* **4**, 615 (2011).
18. C. Jennings, *Fault Activity Map of California and Adjacent Areas, with Locations and Ages of Recent Volcanic Eruptions*, scale 1:750,000, *Geologic Data Map no. 6* (California Division of Mines and Geology, Sacramento, CA, 1994).
19. J. Fletcher, R. Spelz, *Geosphere* **5**, 385 (2009).
20. K. Hudnut, A. Borsa, C. Glennie, J. Minster, *Bull. Seismol. Soc. Am.* **92**, 1570 (2002).
21. Materials and methods are available on *Science* Online.
22. D. A. Lockner, *J. Geophys. Res.* **103**, 5107 (1998).
23. E. Cochran *et al.*, *Geology* **37**, 315 (2009).
24. R. Michel, J. Avouac, *J. Geophys. Res.* **111**, B03408 (2006).
25. A. J. Elliott, J. F. Dolan, D. D. Oglesby, *J. Geophys. Res.* **114**, B02313 (2009).
26. I. Manighetti, M. Campillo, C. Sammis, P. Mai, G. King, *J. Geophys. Res.* **110**, B05302 (2005).
27. C. Marone, C. Scholz, *Geophys. Res. Lett.* **15**, 621 (1988).
28. J. Kaven, S. Martel, *J. Struct. Geol.* **29**, 1463 (2007).
29. E. Kirby *et al.*, *Tectonics* **26**, TC2010 (2007).
30. K. Blisniuk *et al.*, *J. Geophys. Res.* **115**, B08401 (2010).
31. S. Toda, R. Stein, J. Lin, V. Sevilgen, Coulomb 3 stress change modeling software, http://earthquake.usgs.gov/research/modeling/coulomb.

Acknowledgments: LIDAR data acquisition supported by an NSF RAPID grant (EAR-1039168 and 1039147), with additional support from the Southern California Earthquake Center (supported by NSF-EAR-0106924 and U.S. Geological Survey grant 02HQAG0008) and Consejo Nacional de Ciencia y Tecnología (grant CB-2007-81463). Part of this research was supported by NASA's Earth Surface and Interior Focus Area and performed at the Jet Propulsion Laboratory, California Institute of Technology. Y. Fialko, D. Sandwell, J. Galetzka, and A. Gonzalez assisted with Global Positioning System data acquisition and processing. C. Crosby, D. Haddad, O. Kreylos, A. Morelan, and T. Sato provided editorial and computational assistance. The National Center for Airborne Laser Mapping gathered and processed the postevent LIDAR data, distributed at OpenTopography (http://opentopography.org/id/OTLAS.122010.32611.1). We thank INEGI for granting access to the pre-event LIDAR data used for this study. Pre-event LIDAR digital elevation model and derived elevation difference data for the Sierra Cucapah rupture zone are available in the supporting online material.

Supporting Online Material

www.sciencemag.org/cgi/content/full/335/6069/702/DC1
Materials and Methods
Figs. S1 to S4
Table S1
Databases S1 and S2

9 September 2011; accepted 13 January 2012
10.1126/science.1213778

Propagation of Slow Slip Leading Up to the 2011 M_w 9.0 Tohoku-Oki Earthquake

Aitaro Kato,* Kazushige Obara, Toshihiro Igarashi, Hiroshi Tsuruoka, Shigeki Nakagawa, Naoshi Hirata

Many large earthquakes are preceded by one or more foreshocks, but it is unclear how these foreshocks relate to the nucleation process of the mainshock. On the basis of an earthquake catalog created using a waveform correlation technique, we identified two distinct sequences of foreshocks migrating at rates of 2 to 10 kilometers per day along the trench axis toward the epicenter of the 2011 moment magnitude (M_w) 9.0 Tohoku-Oki earthquake in Japan. The time history of quasi-static slip along the plate interface, based on small repeating earthquakes that were part of the migrating seismicity, suggests that two sequences involved slow-slip transients propagating toward the initial rupture point. The second sequence, which involved large slip rates, may have caused substantial stress loading, prompting the unstable dynamic rupture of the mainshock.

Laboratory and theoretical studies have proposed that earthquakes are preceded by a nucleation process where stable, slow rupture growth develops into unstable, high-speed rupture within a confined zone on a fault (*1*–*5*). The nucleation process has been discussed actively in association with the occurrence of foreshocks near the mainshock hypocenters and the presence of short-duration initial phases in the records of some earthquake events (*6*–*10*). A recent study on the 1999 moment magnitude (M_w) 7.6 Izmit, Turkey, earthquake suggested the possibility that the mainshock was preceded, for 44 min, by a phase of slow slip at the base of the brittle crust (*11*). If this kind of premonitory slow-slip behavior also precedes other large earthquakes, its knowledge should have crucial implications for earthquake prediction and risk assessment. It is, therefore, essential to scrutinize seismic records of other large, well-recorded earthquakes in search of similar nucleation processes.

The 11 March 2011 Tohoku-Oki earthquake was the first M_w 9 event to be recorded by a dense network of continuous and broad–frequency-range seismic stations. The extremely large spatial extent of the event (up to ~500 km) is expected to help study how it nucleated, providing an invaluable opportunity to elucidate preparatory processes for earthquake generation. The Tohoku-Oki earthquake ruptured a megathrust fault off the eastern shore of northern Honshu, Japan, where the Pacific plate is subducting beneath a continental plate at a convergence rate of 10 cm/year. According to the Japan Meteorological Agency (JMA) catalog, the mainshock was preceded by foreshock sequences lasting 23 days (*12*), starting with a burstlike seismicity in mid-February. The largest foreshock was a M_w 7.3 event that took

Earthquake Research Institute, The University of Tokyo, Tokyo, Japan.

*To whom correspondence should be addressed. E-mail: akato@eri.u-tokyo.ac.jp

place along the plate interface on 9 March (Fig. 1). The foreshock sequences occurred in proximity to the initiation point of the mainshock rupture and were located near the deepest end of the area of the largest cumulative coseismic slip (*13*). After the M_w 7.3 foreshock, the seismicity from the JMA catalog appeared to migrate toward the mainshock epicenter, which was interpreted as a propagation of afterslip (*14*).

Although the JMA routinely determines hypocenters across the Japanese islands, a large portion of the foreshock sequences is missing from its catalog, mainly because the burstlike seismicity and the aftershocks associated with the M_w 7.3 event tended to be masked by overlapping arrivals of waves from different earthquakes (low signal-to-noise ratios). We therefore applied a matched-filter technique (*15*–*17*) to detect missing events with the use of continuous three-component velocity seismograms recorded at 14 stations along the Pacific coast (Fig. 1) between 13 February and 11 March (*18*). We used all 333 earthquakes in the JMA catalog for the same period as the template events and looked for events that strongly resembled them. The correlation coefficient between a template event waveform and a target waveform was calculated on every component at every station and was averaged throughout. When the mean correlation peak exceeded a threshold level [eight times the standard deviation (*17*)], it was labeled as a positive detection (fig. S1). After removing multiple counts, our matched filter technique identified 1416 events, more than four times the number in the JMA catalog.

In a space-time diagram of all detected events (Fig. 2), we recognize two distinct sequences of earthquake migration in the trench-parallel direction toward the epicenter of the M_w 9.0 mainshock. Both sequences took place between the epicenters of the M_w 7.3 foreshock and the mainshock, and they overlap considerably in space (Fig. 1).We refer to this overlap area as the "earthquake migration zone" (EMZ). The JMA catalog shows a similar pattern, but the migrations are less conspicuous because of the sparser data coverage.

The first migration sequence started in mid-February at a speed of ~2 km/day near the epicenter of the M_w 7.3 foreshock and later sped up to 5 km/day (red dashed lines in Fig. 2). The width of the seismically active zone also expanded slightly with time in the trench-parallel direction. This pattern could be explained by a succession of several independent afterslip sequences, each associated with a moderate earthquake (*19*). The whole migration sequence, which stopped in late February near the mainshock epicenter, was followed by a lull in foreshock activities that lasted for ~8 days.

A second migration sequence broke out just after the M_w 7.3 foreshock at an average speed of ~10 km/day. Its migration front, slowing down with time, is well approximated by a parabolic curve describing a diffusive process (*14*). Seismic activities in the EMZ, corresponding to the second migration sequence, peaked at a delay of about half a day after the M_w 7.3 foreshock. The northern part (outside the EMZ) saw an immediate, abrupt increase in the number of earthquakes, which decreased with time monotonically, according to the modified Omori law (Fig. 2).

About 90% of all migrating Tohoku-Oki foreshocks with moderate-to-large magnitudes located within the EMZ had low-angle thrust faulting mechanisms similar to the mainshock. They also included small repeating earthquakes that had identical mechanisms and identical locations (denoted by red stars in Figs. 1 and 2) (*18*), which are considered to be recurrent ruptures on potentially seismic patches of a fault to overtake quasi-static slip in the aseismically creeping areas outside (*20*–*23*). Therefore, the most plausible explanation for these migration sequences is the propagation of slow-slip events within the EMZ along the plate interface toward the initiation point of the M_w 9.0 mainshock rupture. The slow-slip migration speeds of 2 to 10 km/day are comparable to those of episodic-tremor and slow-slip events found along deeper extensions of warm subduction zones (*24*, *25*). This also supports our interpretation of the foreshock migration as propagation of slow slip.

We next estimated the time history of interplate slipping induced by slow-slip transients along the plate interface based on the analysis of the small repeating earthquakes. We identified the repeating earthquakes, applying the same technique as used in a previous study (*23*), to the JMA catalog (red stars in Fig. 2) (*18*). The slip in each event was calculated based on a unique scaling relation between the seismic moment and the fault slip for repeating earthquakes (*20*). The slip estimates were totaled within each of the four regional divisions shown in Fig. 3A, and the sum was divided by the number of repeating earthquake sequences within the corresponding division. In addition, our matched-filter technique enabled us to detect many events that were found to resemble the repeating earthquakes (green stars in Fig. 2). They are located in the close vicinity of, but not exactly on, fault patches where the corresponding repeating earthquakes occur. Their activities may provide a clue to the time evolution of aseismic creep outside the seismic patches (Fig. 3B).

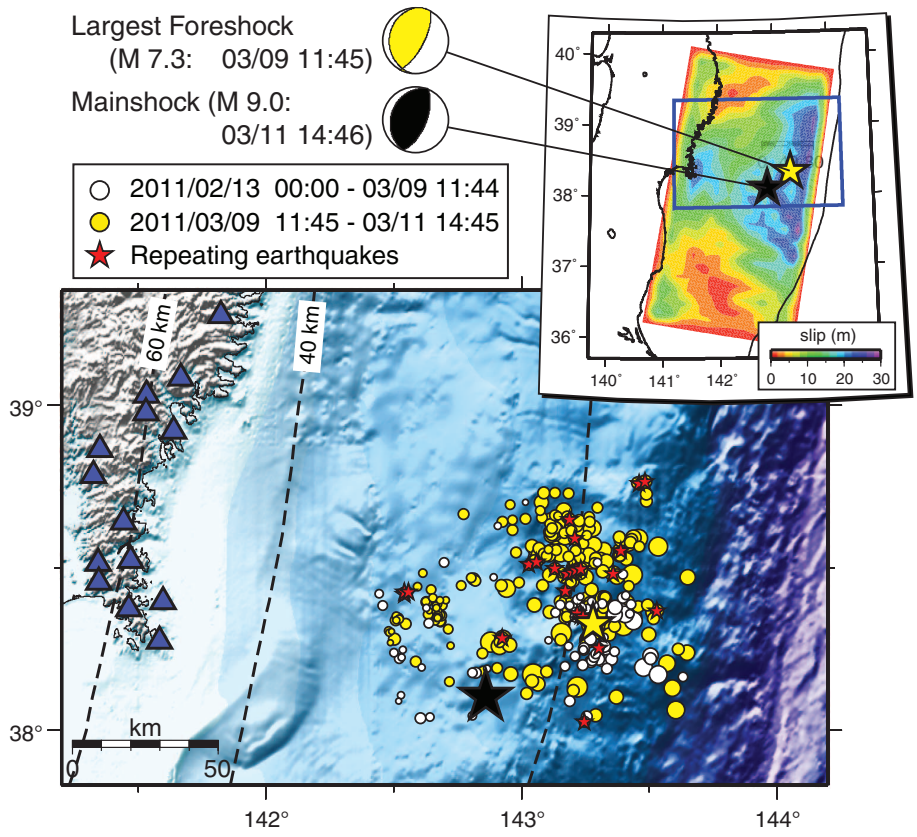

Fig. 1. Foreshocks and the mainshock rupture. Map of the foreshock region of the 2011 Tohoku-Oki earthquake, including the epicenters of the 11 March M_w 9.0 mainshock (black star), the 9 March M_w 7.3 largest foreshock (yellow star), and all 333 events in the JMA catalog between 13 February and 11 March 2011 (white and yellow circles scaled to magnitude). Blue triangles, seismic stations; dashed lines, iso-depth contours of the plate boundary at 20-km intervals (*34*); red stars, epicenters of small repeating earthquakes in the JMA catalog, identified as such based on a previous study (*23*). (**Inset**) Distribution of the total mainshock slip, imaged by a finite-source modeling using global broadband seismograms (*13*). Yellow/white and black/white spheres denote focal mechanisms of the largest foreshock and the mainshock, respectively.

Transient slip first started to build up to the south of the M_w 7.3 epicenter (divisions c and d in Fig. 3B) and continued to do so from mid- to late February at speeds far larger than the plate convergence rate. This increase in the slip rates coincided with the first sequence of earthquake migration toward the epicenter of the M_w 9.0 mainshock. After the M_w 7.3 foreshock, the amount of transient slip increased abruptly to the north of the M_w 7.3 epicenter, though it slightly slowed down logarithmically with time (a to c in Fig. 3B), a phenomenon commonly observed in afterslip following M_w 7 to 8 plate-interface earthquakes along the Japan and Kuril trenches (*26*–*28*). Within the EMZ, in contrast, slip increased at a rate of ~6 mm/hour, or up to 600 times the plate convergence rate (V_{pl}), during that final phase (c and d in Fig. 3B). Thus, the current study provides strong evidence for the propagation of slow-slip events toward the M_w 9.0 epicenter, based on the two sequences of earthquake migration accompanied by the repeating earthquakes.

The cumulative slip before the M_w 9.0 mainshock averaged ~20 cm across all four regional divisions. This converts to an estimated total moment release by the slow-slip transients worth up to M_w ~7.1, assuming that a fault with a 90–by–90-km^2 dimension (comparable to the foreshock region) slipped homogeneously (rigidity: 30 GPa). This assumption means that both seismic and aseismic slip coexisted on this fault. Geodetic measurements on land (Global Positioning System) detected transient deformation after the M_w 7.3 foreshock (*29*), whose moment release roughly coincided with that estimated in this study. This is consistent with the presence of the second slow-slip sequence documented in this study, although the geodetic measurements were not able to recognize their propagation toward the mainshock hypocenter because the land-based geodetic instruments are not sensitive to small amounts of off-shore fault slip.

The M_w 7.3 foreshock occurred near the northern end of the EMZ after the first migration of slow slip toward the M_w 9.0 mainshock hypocenter. In contrast, the mainshock nucleated near the southern end of the EMZ after the second migration, which was faster than the first one. Interestingly, the propagation of slow slip stopped in both cases near the mainshock hypocenter (Fig. 2). This suggests that the initiation point of the mainshock rupture was resistive enough to withstand the stress concentration caused by the oncoming slow-slip transients. A recent numerical modeling of the Tohoku-Oki earthquake also indicated that a shallow, highly resistive patch should be present close to the foreshock area to generate a M_w 9 earthquake (*30*).

The propagation of slow slip could be interpreted as part of the nucleation process, but there was no power-law acceleration in the slip and rupture growth to the mainshock origin of the type predicted by preslip models (*1*–*5*). In addition, the mainshock was not preceded by accelerating occurrences of foreshocks close to the mainshock hypocenter as reported for the 1999 Izmit earthquake (*11*). It should nevertheless be noted that the second sequence of slow slip had much larger slip rates and a larger migration speed than the first sequence (Figs. 2 and 3).

The slip rates involved in the second sequence of slow slip were also larger than those previously reported for transient slip after other earthquakes. In fact, the second sequence released approximately one-half of the moment of the M_w 7.3 Tohoku-Oki foreshock in only 2 days (*29*). In contrast, slow-slip transients (afterslip) after previous M_w 7 to 8 earthquakes along the Japan and Kuril trenches had slip rates of less than 4 cm/day (150 times the V_{pl}) during the first few days (*27*, *31*) and needed more than a few months to release half the moment of the mainshock (six events in table S1) (*26*, *32*).

It is conceivable that the first sequence of slow slip in the Tohoku-Oki focal region had weakened the plate interface within the EMZ,

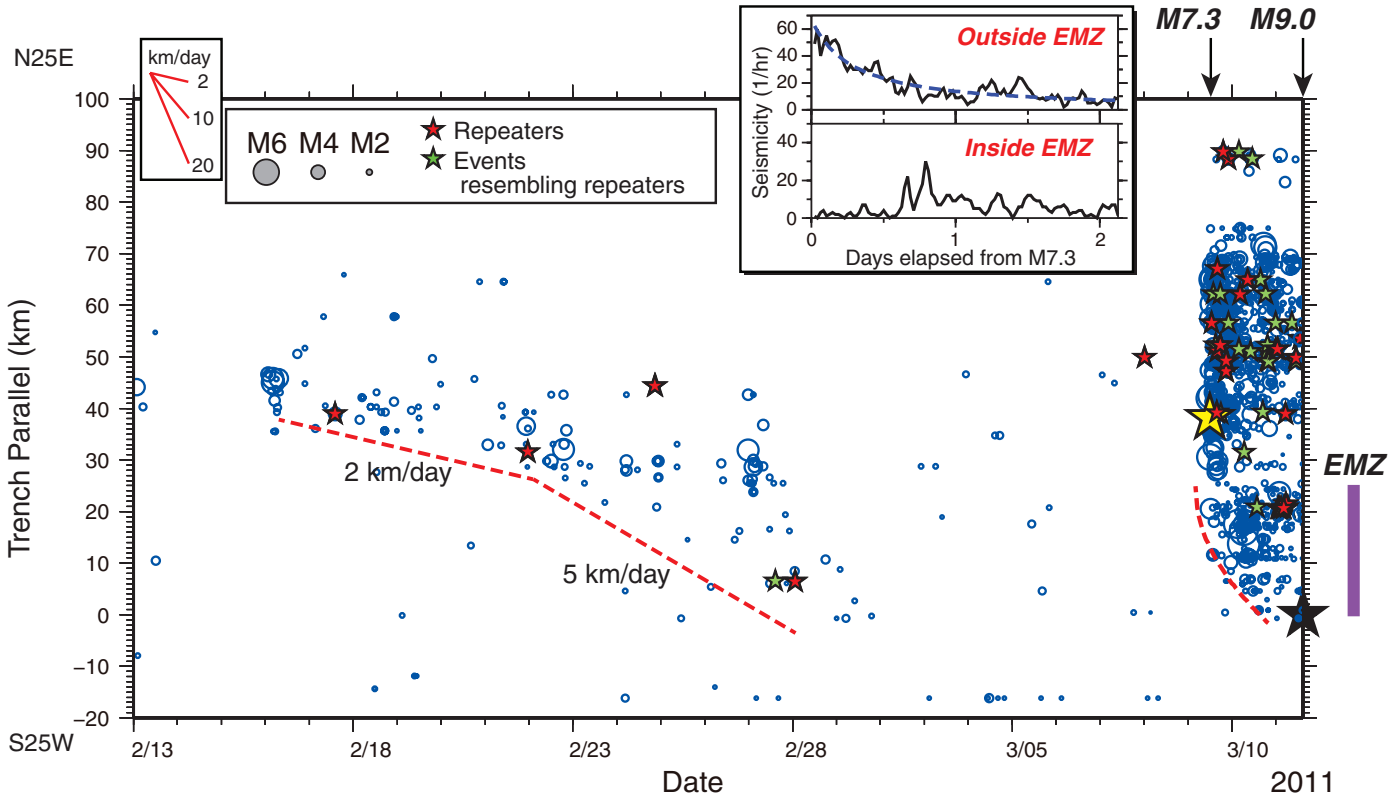

Fig. 2. Earthquake migration toward the rupture initiation point of the mainshock. Space-time diagram of all detected events between 13 February and the mainshock origin time, with earthquake origin locations indicated in terms of the distance along the trench axis (blue circles scaled to magnitude). Red dashed lines, approximate locations of the fronts of earthquake migration; red stars, repeating earthquakes in the JMA catalog (*23*); green stars, newly detected events that were found to resemble those repeating events; black star, M_w 9.0 mainshock; yellow star, M_w 7.3 largest foreshock. (**Inset**) Time variations in seismicity rates inside and outside the EMZ after the M_w 7.3 largest foreshock. The blue dashed curve denotes the least-squares fitting of the modified Ohmori law.

which facilitated slip (*33*). A subsequent, second sequence of slow slip, which had large slip rates, may have caused substantial stress loading onto the prospective hypocenter of the M_w 9.0 mainshock and prompted the initiation of unstable dynamic rupture there.

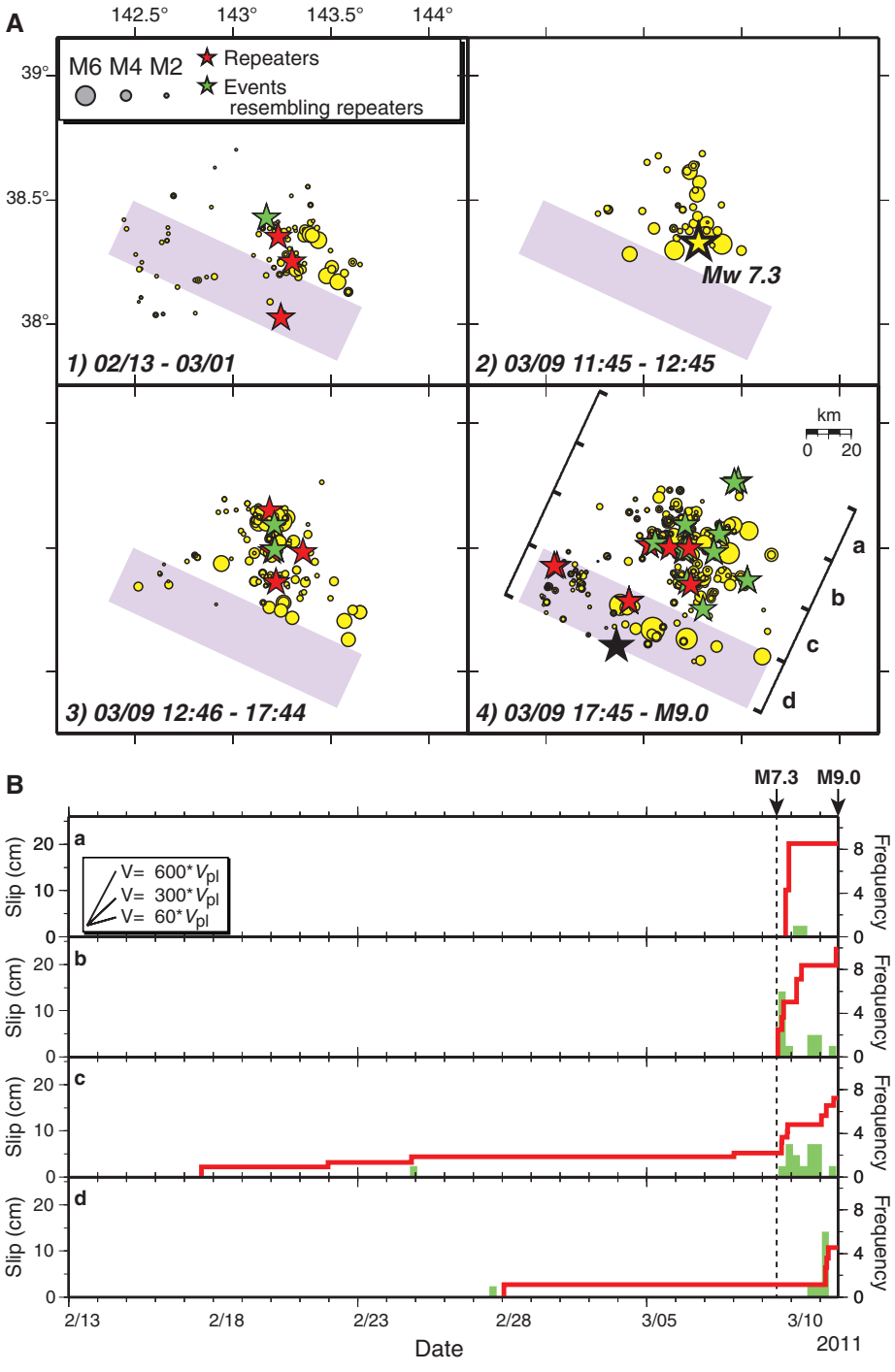

Fig. 3. Space-time characteristics of the two sequences of migrating slow-slip transients. (**A**) Map of all detected earthquakes (yellow circles scaled to magnitude) in different time windows. Red stars, repeating earthquakes in the JMA catalog; green stars, newly detected events that were found to resemble the repeating events; black star, M_w 9.0 mainshock; yellow star, M_w 7.3 largest foreshock; light purple rectangles, EMZ as defined in this study. (**B**) Average cumulative quasi-static slip in each of the four regional divisions shown in (A), plotted against time from 13 February to the mainshock origin (red lines). Green bars, combined frequencies, in successive 6-hour intervals, of newly detected events that were found to resemble repeating earthquakes; Black vertical dashed line, occurrence time of the largest foreshock. Line segments in the inset denote slopes corresponding to 60, 300, and 600 times the plate convergence rate.

References and Notes

1. J. H. Dieterich, *J. Geophys. Res.* **84**, 2161 (1979).
2. M. Ohnaka, *Tectonophysics* **211**, 149 (1992).
3. B. Shibazaki, M. Matsu'ura, *Geophys. Res. Lett.* **19**, 1189 (1992).
4. M. Ohnaka, L. Shen, *J. Geophys. Res.* **104**, 817 (1999).
5. N. Lapusta, J. R. Rice, Y. Ben-Zion, G. Zheng, *J. Geophys. Res.* **105**, 23765 (2000).
6. D. A. Dodge, G. C. Beroza, W. L. Ellsworth, *J. Geophys. Res.* **101**, 22371 (1996).
7. W. L. Ellsworth, G. C. Beroza, *Science* **268**, 851 (1995).
8. J. Mori, H. Kanamori, *Geophys. Res. Lett.* **23**, 2437 (1996).
9. R. E. Abercrombie, J. Mori, *Nature* **381**, 303 (1996).
10. J. J. McGuire, M. S. Boettcher, T. H. Jordan, *Nature* **434**, 457 (2005).
11. M. Bouchon *et al.*, *Science* **331**, 877 (2011).
12. F. Hirose, K. Miyaoka, N. Hayashimoto, T. Yamazaki, M. Nakamura, *Earth Planets Space* **63**, 513 (2011).
13. S. Ide, A. Baltay, G. C. Beroza, *Science* **332**, 1426 (2011).
14. R. Ando, K. Imanishi, *Earth Planets Space* **63**, 767 (2011).
15. D. R. Shelly, G. C. Beroza, S. Ide, *Nature* **446**, 305 (2007).
16. Z. Peng, P. Zhao, *Nat. Geosci.* **2**, 877 (2009).
17. N. Aso, K. Ohta, S. Ide, *Geophys. Res. Lett.* **38**, L08303 (2011).
18. Materials and methods are available as supporting material on *Science* Online.
19. T. Matsuzawa, N. Uchida, T. Igarashi, T. Okada, A. Hasegawa, *Earth Planets Space* **56**, 803 (2004).
20. R. M. Nadeau, L. R. Johnson, *Bull. Seismol. Soc. Am.* **88**, 790 (1998).
21. Z. Peng, Y. Ben-Zion, *Geophys. J. Int.* **160**, 1027 (2005).
22. T. Chen, N. Lapusta, *J. Geophys. Res.* **114**, B01311 (2009).
23. T. Igarashi, *Geophys. Res. Lett.* **37**, L20304 (2010).
24. H. Dragert, K. Wang, T. S. James, *Science* **292**, 1525 (2001).
25. K. Obara, *J. Geophys. Res.* **115**, B00A25 (2010).
26. K. Heki, S. Miyazaki, H. Tsuji, *Nature* **386**, 595 (1997).
27. S. Miyazaki, P. Segall, J. Fukuda, T. Kato, *Geophys. Res. Lett.* **31**, L06623 (2004).
28. N. Uchida *et al.*, *Gondwana Res.* **16**, 527 (2009).
29. S. Miyazaki, J. J. McGuire, P. Segall, *Earth Planets Space* **63**, 637 (2011).
30. N. Kato, S. Yoshida, *Geophys. Res. Lett.* **38**, L00G04 (2011).
31. Y. Yagi, M. Kikuchi, T. Nishimura, *Geophys. Res. Lett.* **30**, 2177 (2003).
32. H. Suito, T. Nishimura, M. Tobita, T. Imakiire, S. Ozawa, *Earth Planets Space* **63**, 615 (2011).
33. H. Houston, B. G. Delbridge, A. G. Wech, K. C. Creager, *Nat. Geosci.* **4**, 404 (2011).
34. J. Nakajima, A. Hasegawa, *Geophys. Res. Lett.* **33**, L16309 (2006).

Acknowledgments: We thank M. Nakatani for helpful comments and suggestions and the National Research Institute for Earth Science and Disaster Prevention, Tohoku Univ., and JMA for allowing us to use waveform data from their permanent stations. JMA provided us with an earthquake catalog. This study was supported by the Ministry of Education, Culture, Sports, Science and Technology of Japan, under its Observation and Research Program for Prediction of Earthquakes and Volcanic Eruptions.

Supporting Online Material

www.sciencemag.org/cgi/content/full/science.1215141/DC1
Materials and Methods
Fig. S1
Table S1
References (*35*–*37*)

11 October 2011; accepted 6 January 2012
Published online 19 January 2012;
10.1126/science.1215141

Propagation of Slow Slip Leading Up to the 2011 M_W 9.0 Tohoku-Oki Earthquake

Aitaro Kato, Kazushige Obara, Toshihiro Igarashi, Hiroshi Tsuruoka, Shigeki Nakagawa and Naoshi Hirata (January 19, 2012)
Science **335** (6069), 705-708. [doi: 10.1126/science.1215141]
originally published online January 19, 2012

Editor's Summary

Before Tohoku-Oki

Recordings by Japan's dense seismic network in the days and weeks before the 2011 M_W 9.0 Tohoku-Oki earthquake provide an opportunity to interrogate what caused the dynamic rupture of one of the largest earthquakes on record. Using a method to extract small earthquakes that are often obscured by overlapping seismic waves, **Kato *et al.*** (p. 705, published online 19 January) identified over a thousand small repeating earthquakes that migrated slowly toward the hypocenter of the main rupture. Based on the properties of these foreshocks, the plate interface experienced two sequences of slow slip, the second of which probably contributed a substantial amount of stress and may have initiated the nucleation of the main shock.

Science (print ISSN 0036-8075; online ISSN 1095-9203) is published weekly, except the last week in December, by the American Association for the Advancement of Science, 1200 New York Avenue NW, Washington, DC 20005.